



Spectrum, lifetime distributions and relaxation in a dimer with strong excitonic–vibronic coupling

Christiane Koch, Bernd Esser*

Institut für Physik, Humboldt-Universität zu Berlin, Invalidenstr. 110, D-10115 Berlin, Germany

Received 26 May 1998; received in revised form 4 November 1998; accepted 8 November 1998

Abstract

The fine structure of the complex quantum spectrum of a dimer constituted by monomers with a finite lifetime in the excited states and a strong excitonic–vibronic coupling has been investigated in detail. Lifetime distributions of the spectrum are analysed for different system parameter sets. It is shown that in case of an asymmetric configuration the spectrum may be characterised by a broad distribution of the lifetimes of the eigenstates. This can give rise to a strongly varying relaxation behaviour, which is due to the mixing of the monomer spectra with two different excitonic lifetimes in the dimer spectrum. © 1999 Elsevier Science B.V. All rights reserved.

Keywords: Dimers; Relaxation dynamics; Exciton–phonon interaction; Quenching

1. Introduction

The coupling between excited states and vibronic degrees of freedom of the environment is a basic mechanism that influences transfer and relaxation properties in molecular systems. In the case of a bath of oscillators, the implications of this coupling for the excitation propagation have been intensively studied (see, e.g. Ref. [1]) and extended to include relaxation effects such as the interplay between propagation and quenching [2]. In the last years there is, however, a growing interest in the properties of a nonlinear situation when the excited states strongly couple to selected vibrational modes. A dimer model describing the nonlinear properties of excited states strongly coupled to

a single vibrational mode has been investigated ([3,4,8] and references therein). In the full quantum description of this dimer model one finds that the spectrum displays features intermediate between regular and irregular structures [5]. These features of the spectrum have been characterised as “incipience of quantum chaos”. In this case the spectrum is very sensitive to changes of the system parameters.

In this paper we demonstrate the sensitive dependence on the parameters by extending the dimer model to the asymmetric case and to finite lifetimes of the excitations. We consider complex excitation energies with an imaginary part describing the finite lifetime. The finite lifetime or decay rate is due to some excitation quenching or relaxation mechanism inside the monomers, which removes the excitation from the excited transfer states. We note that electron or excitation transfer related to optical properties has been experimentally studied in the

*Corresponding author. Tel.: + 49 30 2093 7636; fax: + 49 30 2093 7638; e-mail: besser@physik.hu-berlin.de.

presence of quenching, e.g. in porphyrin based molecular compounds linked to a benzoquinone quencher molecule [6]. We show that for an asymmetric dimer and a strong coupling of the excitation to the vibrational mode a broad intrinsic lifetime or decay rate distribution in the complex eigenstates of the dimer may occur. As a consequence strongly varying relaxation behaviour is obtained.

2. Model

We consider a dimer described by the Hamiltonian

$$\hat{H} = \sum_n (\tilde{\varepsilon}_n + \gamma_n q_n) |n\rangle \langle n| + \sum_{\substack{n, m \\ n \neq m}} V_{nm} |n\rangle \langle m| + \sum_n \frac{1}{2} (p_n^2 + \omega_n^2 q_n^2), \quad (1)$$

where $|n\rangle$ ($|m\rangle$) is the exciton state at the n th (m th) molecule with the on-site energy $\tilde{\varepsilon}_n$, γ_n the exciton–phonon coupling constant and V_{nm} the transfer matrix element, $n, m = 1, 2$. The variables of the intramolecular vibrations of the two monomers constituting the dimer are q_n , p_n and ω_n representing coordinate, momentum and frequency, respectively. We will assume the case of symmetric transfer rates, $V_{nm} = V_{mn} = -V$, $V > 0$, equal coupling constants, $\gamma_1 = \gamma_2 = \gamma$, and equal intramolecular frequencies, $\omega_1 = \omega_2 = \omega$. By introducing normal modes, the intramolecular vibrations can be reduced to a single mode since only the relative displacement is coupled to the excitation. Excitation quenching on the monomers of the dimer is modelled by complex site energies, $\tilde{\varepsilon}_n = \varepsilon_n - i\Gamma_n$, where the real part ε_n denotes the excitation energy and Γ_n denotes the decay rate or inverse lifetime due to an excitation quenching or relaxation mechanism. Passing to dimensionless variables by measuring the energy in units of $2V$, $\mathbf{H} = \mathbf{H}/2V$, ($\hbar = 1$), one obtains

$$\hat{\mathbf{H}} = (\varepsilon_+ - i\Gamma_+) \hat{1} + (\varepsilon_- - i\Gamma_-) \hat{\sigma}_z - \frac{1}{2} \hat{\sigma}_x + \frac{1}{2} (P^2 + r^2 Q^2) \hat{1} + \sqrt{\frac{p}{2}} r Q \hat{\sigma}_z. \quad (2)$$

Here $\hat{\sigma}_i$ are the standard Pauli-matrices, $i = x, z$, and we use the spin representation of the two-site system representing the monomer states $|1\rangle$ and $|2\rangle$ by the spin up and spin down states, respectively. The dimensionless relative displacement and the corresponding momentum are $Q = \sqrt{2V}(q_1 - q_2)$ and $P = (p_1 - p_2)/\sqrt{2V}$. The Hamiltonian (2) depends on the parameters

$$p = \frac{\gamma^2}{2V\omega^2}, \quad (3)$$

$$r = \frac{\omega}{2V}, \quad (4)$$

$$\varepsilon_{\pm} = \frac{1}{4V} (\varepsilon_1 \pm \varepsilon_2), \quad (5)$$

$$\Gamma_{\pm} = \frac{1}{4V} (\Gamma_1 \pm \Gamma_2). \quad (6)$$

The parameter p expresses the coupling strength of the excitation to the vibration, and r is the adiabatic parameter. The sums ε_+ and Γ_+ represent the centre of mass of the excitation band and relaxation rates, whereas the differences ε_- and Γ_- are asymmetry parameters. We note that the symmetric case with equal decay rates on the monomers, i.e. $\Gamma_1 = \Gamma_2 = \Gamma$, ($\Gamma_+ = \Gamma$, $\Gamma_- = 0$), results in the same decay rate Γ for all dimer states. Therefore we considered the nontrivial case $\Gamma_- \neq 0$.

We found it useful to consider the formation of the spectrum of Eq. (2) as the result of a mixing of adiabatic reference states connected with the adiabatic potentials. These potentials are calculated in a standard way by solving the Q -dependent eigenvalue problem for the adiabatic part of Eq. (2). One finds the two adiabatic potentials $U_{\text{ad}}^{\pm}(Q)$ for the upper (+) and lower (−) adiabatic states,

$$U_{\text{ad}}^{\pm}(Q) = \frac{r^2}{2} Q^2 \pm \sqrt{\frac{1}{4} + \left(\varepsilon_- - i\Gamma_- + \sqrt{\frac{p}{2}} r Q \right)^2}. \quad (7)$$

The potentials $U_{\text{ad}}^{\pm}(Q)$ are complex due to the asymmetry Γ_- in the decay rates, in Eq. (7) the origin of

the complex energy plane was shifted to $\varepsilon_+ - i\Gamma_+$ (the real parts of Eq. (7) are the adiabatic potentials while the imaginary parts of Eq. (7) can be viewed as the Q -dependent lifetimes of the adiabatic states). Introducing the Hamiltonians of the adiabatic reference systems associated with $U_{\text{ad}}^{\pm}(Q)$, the formation of the spectrum of Eq. (2) can now be understood as a mixing of the two adiabatic reference systems which is produced by the nonadiabatic couplings. Although a quantitative investigation of the role of the nonadiabatic couplings over the range of all the parameters and a broad energy interval is not feasible, we will discuss the manifestations of these couplings in the structure of the complex spectrum from a qualitative point of view.

3. Results

3.1. Spectrum and decay rates

We investigated the fine structure of the complex spectrum of the Hamiltonian Eq. (2) by numerical diagonalisation in a spin-oscillator product basis. The oscillator states were represented by standard Hermitian polynomials and the spin states were represented by the eigenstates of $\hat{\sigma}_z$. The dimension of the matrix ranged from $N = 1000$ in the symmetric case to $N = 3000$ for the asymmetric case, the first 700–1000 eigenvalues and eigenstates were used in the analysis. Different values of the parameters p, r as well as the asymmetry parameters ε_- and Γ_- were considered. The parameters ε_+ and Γ_+ only cause a rigid shift of all the eigenvalues in the complex plane, they are irrelevant for the structure of the spectrum. We therefore rescaled the spectrum by shifting ε_+ and Γ_+ to the origin. We note that the decay rates obtained for a given value of Γ_- are representative for all different Γ_1 and Γ_2 having one and the same value of Γ_- . For a given Γ_- , the actual decay rates of the eigenstates are easily found by adding Γ_+ to the imaginary parts of the complex eigenvalues.

Analysing the complex eigenvalue plane we found that the ranges of the asymmetry parameters ε_- and Γ_- can be divided into the following

characteristic regions:

(A) Small values of the asymmetry parameters: $\varepsilon_- = 0, \Gamma_- \ll 1$.

(B) Intermediate / large values of the site energy asymmetry and small values of the lifetime asymmetry: $\varepsilon_- \sim 0.1, \dots, 1/\varepsilon_- > 1$ and $\Gamma_- \ll 1$.

(C) Arbitrary values of the site energy asymmetry ε_- and intermediate large/values of the lifetime asymmetry: $\Gamma_- \sim 0.1, \dots, 1/\Gamma_- > 1$.

In case (A) the effect of the asymmetry upon the lifetimes is negligibly small: The majority of the numerically obtained decay rates are close to zero with a few scattered off. An example for this type of behaviour is given in Fig. 1a. This situation can also be understood from a perturbational point of view: Considering the whole asymmetric part in the Hamiltonian Eq. (2) as a perturbation of the symmetric case, one finds that in first order perturbation theory the asymmetry is proportional to the occupation difference z of the monomers, which vanishes for the eigenstates of a symmetric dimer.

In case (C) the decay rate asymmetry results in a splitting of the lifetimes into two branches located around the values $\pm \Gamma_-$, i.e. the spectrum of decay rates is close to the values Γ_1, Γ_2 of the monomers (taking into account the rigid shift by Γ_+). This behaviour of the spectrum of decay rates is illustrated in the complex eigenvalue spectrum of Fig. 1b for $\Gamma_- = 1$ (decay rate asymmetry is twice the transfer matrix element). The obtained rates are almost equal to the unperturbed monomer values over the complete energy range. From Fig. 1c it can be seen that the formation of two well separable branches of decay rates starts with the intermediate value $\Gamma_- = 0.05$. The splitting of the spectrum of decay rates into two branches approaching the lifetimes of the monomers can be interpreted as follows: For a strong asymmetry, the decay rate at least at one of the monomers becomes greater than the transfer rate, i.e. the transfer is suppressed due to the fast decay. Then no substantial mixing of the monomer spectra by the transfer can be expected, i.e. the spectrum approaches that of the isolated integrable monomers.

We now turn to the results of case (B) for which we obtained nontrivial lifetime distributions. Typical results of complex eigenvalue spectra obtained

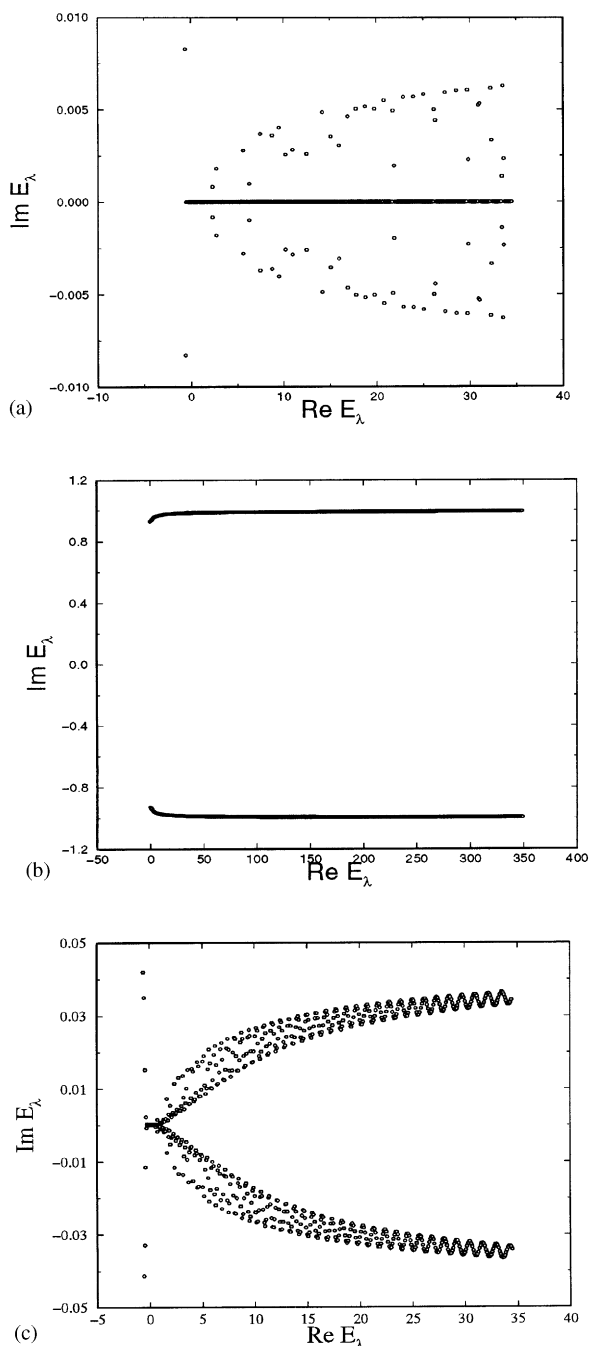


Fig. 1. Complex eigenvalue spectra E_λ illustrating cases (A) and (C). (a) Case A – small asymmetry. The parameters are $p = 2$, $r = 0.1$, $\varepsilon_- = 0$, $\Gamma_- = 0.01$. In the complex plane of the eigenvalues E_λ , the majority of decay rates (the imaginary parts of the E_λ) are close to zero. (b) Case C – large lifetime asymmetry, the

for different parameters p , r and ε_- , but one and the same small asymmetry value $\Gamma_- = 0.01$ are represented in Figs. 2–4.

In Fig. 2 the complex eigenvalue spectrum is presented for intermediate coupling, $p = 2$, and intermediate asymmetry, $\varepsilon_- = 0.5$. As can be seen from Fig. 2, for this case the decay rates have moved away from zero forming two strands with a pattern of transitions between them. Note the difference to case C in Fig. 1b where the two branches are close to the value of Γ_- , whereas in the present case the mean values of the decay rates in the strands are an order of magnitude smaller than Γ_- . The two strands of lifetimes are located in the region where the lower and the upper adiabatic potentials, $U_{ad}^-(Q)$ and $U_{ad}^+(Q)$, overlap. One can understand the formation of these strands as due to a mixing of the complex adiabatic eigenstates associated with $U_{ad}^-(Q)$ and $U_{ad}^+(Q)$. This mixing is produced by the nonadiabatic couplings and it is a signature of nonintegrability and chaos of the system, as can be shown by considering the mixed quantum–classical dynamics deduced from the Hamiltonians Eq. (1), Eq. (2) [3,5].

This interpretation is confirmed by the analysis of the complex eigenvalue spectrum in Fig. 3a for a case with strong coupling, $p = 50$, but otherwise the same parameters as in Fig. 2. Part of the decay rates has shifted away from zero and now fills the complex plane up to values of the order of the input parameter Γ_- . However, most of the rates are close to zero, which is due to the relatively small asymmetry parameter in this case. Again we point out the close relation of the complex spectrum to the adiabatic potentials (shown in Fig. 3b): The spread in the decay rates starts at an energy equal to the minimum of the upper adiabatic potential. In order to illustrate that the mixing starts indeed in the region of the minimum of the upper potential

← parameters are $p = 2$, $r = 1.0$, $\varepsilon_- = 0.01$, $\Gamma_- = 1$. A complete splitting of the decay rates in the E_λ -plane into two branches at $\Gamma_- = \pm 1$ has occurred. (c) Transition to the case C – formation of two branches in the distribution of the decay rates for intermediate values of the lifetime asymmetry. The parameters are $p = 2$, $r = 0.1$, $\varepsilon_- = 0.01$, $\Gamma_- = 0.05$.

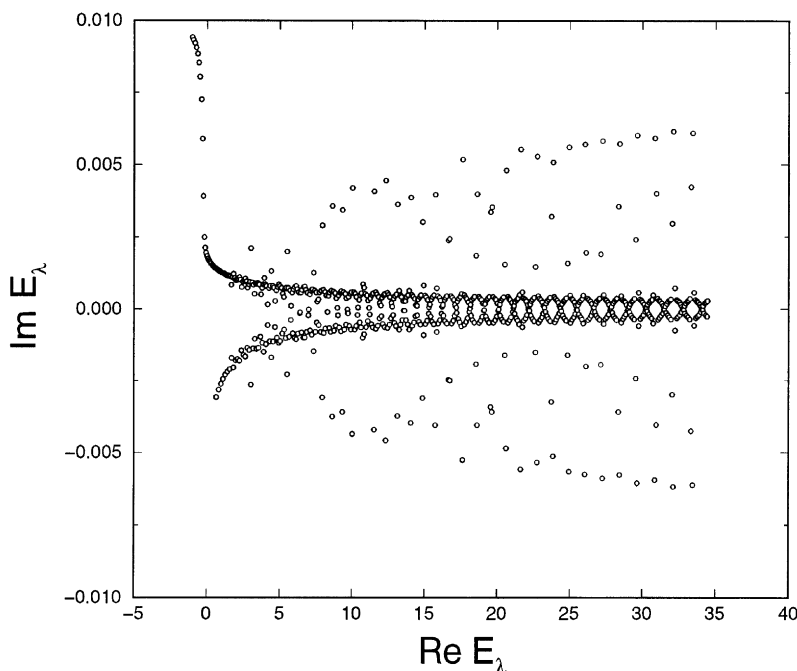


Fig. 2. Case B – Complex eigenvalue spectrum E_λ for intermediate coupling and asymmetry. The parameters are $p = 2, r = 0.1, \varepsilon_- = 0.5, \Gamma_- = 0.01$. It can be seen how the decay rates move away from zero forming two branches with a pattern of transitions between them.

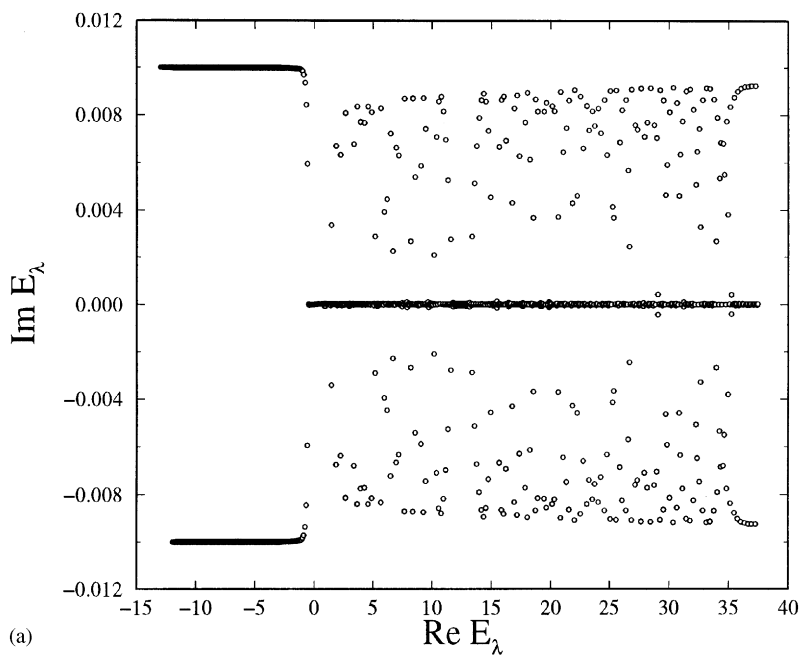
$U_{\text{ad}}^+(Q)$, in Fig. 3a the numerical results for the region below this minimum are displayed as well. The two branches, into which the decay rate spectrum below this minimum separates, are due to the lower adiabatic potential $U_{\text{ad}}^-(Q)$. This separation can also be found by a simple calculation: For the small value of Γ_- , $\Gamma_- = 0.01$, one can approximate the square root in Eq. (7). One finds in first order of Γ_- , that $\text{Im } U_{\text{ad}}^-(Q) = \Gamma_- \text{ sign } Q$, i.e. the decay rates due to the single potential are given by $\pm \Gamma_-$. This confirms that the structure in the decay rates of Fig. 3a is due to the mixing of states in the overlap region of the two potentials.

Finally, in Fig. 4, the decay rates are presented for a strong coupling, $p = 20$, and a large asymmetry, $\varepsilon_- = 10$. Below the minimum of the upper adiabatic potential we observe a regular structure as in Fig. 3. Immediately above the minimum of the upper potential we find a broad distribution of the decay rates which have completely moved away from zero and fill the complex plane more

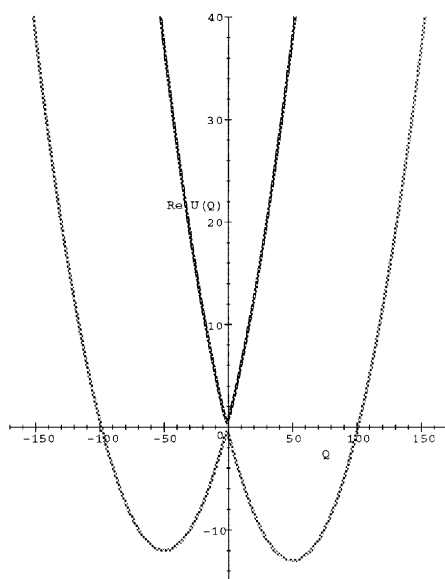
homogenously than the decay rates in Fig. 3a. However, small regular structures are still embedded in the distribution.

3.2. Relaxation

For the calculation of the relaxation we chose the particular case of an asymmetric dimer with a quenching rate placed at one of the monomers of the dimer only, $\Gamma_1 = \Gamma$ and $\Gamma_2 = 0$. In this case $\Gamma_+ = \Gamma_- = \Gamma/4V$, i.e. the spectrum of the complex rates as displayed in the figures of the preceding section has to be shifted up by the value $\Gamma_+ = \Gamma/4V$ in the complex plane in order to obtain the particular decay rates. We note that for this configuration the lower part of the distribution of decay rates is located immediately above zero, i.e. states with particularly small decay rates or long lifetimes are generated. We checked that all the numerically obtained states have a positive decay rate.



(a)



(b)

Fig. 3. Case B – Complex eigenvalue spectrum E_λ (a) for intermediate asymmetry, but large coupling, $p = 50$, with the other parameters as in Fig. 2 ($r = 0.1$, $\varepsilon_- = 0.5$, $\Gamma_- = 0.01$). A substantial part of the decay rates has moved away from zero and fills the complex plane up to values of the order of $\Gamma_- = 0.01$. In (b) the adiabatic potentials are plotted for the selected parameters. The spread of the decay rates due to mixing of the reference systems starts above the energy corresponding to the minimum of the upper adiabatic potential.

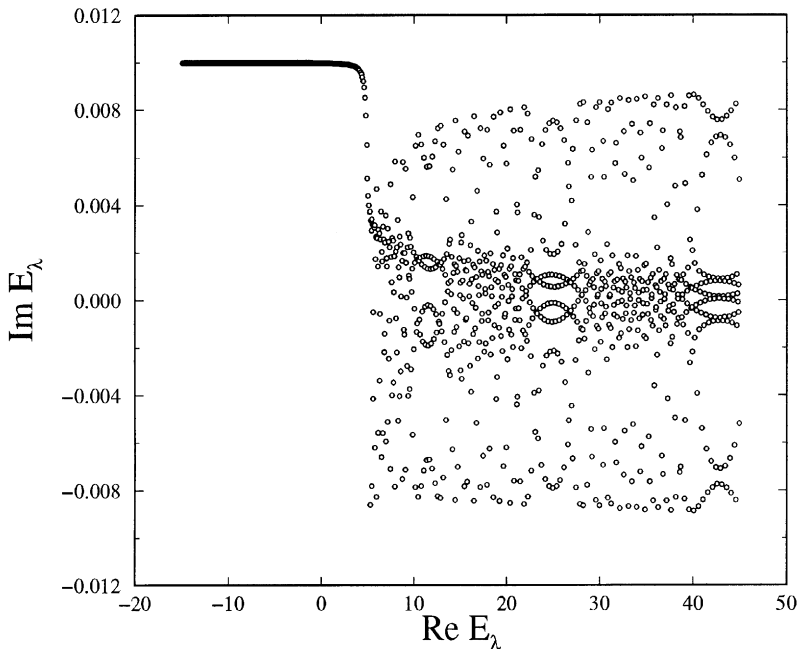


Fig. 4. Case B – Complex eigenvalue spectrum E_λ for large asymmetry and large coupling. The parameters are $p = 20$, $r = 0.1$, $\varepsilon_- = 10$, $\Gamma_- = 0.01$. Above the minimum of the upper adiabatic potential a broad distribution of decay rates with small regular structures embedded can be seen.

To investigate the relaxation behaviour, we computed the expectation value $\langle R(t) \rangle = \langle \Psi(t) | \Psi(t) \rangle$ of the total occupation probability from the state vector $|\Psi(t)\rangle$. As initial states $|\Psi(0)\rangle$ wave packet states of the form

$$|\Psi(0)\rangle = \sum_{\lambda=0} |E_\lambda\rangle \langle E_\lambda | Q, P, a_+, a_- \rangle \equiv \sum_{\lambda=0} e_\lambda |E_\lambda\rangle \quad (8)$$

were prepared. Here $|E_\lambda\rangle$ are the eigenstates of the Hamiltonian Eq. (2). The states $|Q, P, a_+ a_- \rangle$ are product states, $|Q, P, a_+ a_- \rangle = |Q, P\rangle |a_+, a_- \rangle$. Here the oscillator part $|Q, P\rangle$ is a Gaussian wave packet with expectation values Q and P for coordinate and momentum, $|a_+, a_- \rangle$ constitutes the spin part fixing the exciton amplitudes, a_+ and a_- are the occupation probabilities of the left or right monomer in the dimer, respectively. Then the state vector was propagated in time according to

$$|\Psi(t)\rangle = \sum_{\lambda=0} e^{-iE_\lambda t} |E_\lambda\rangle \langle E_\lambda | Q, P, a_+, a_- \rangle, \quad (9)$$

where E_λ is the complex eigenvalue of the eigenstate $|E_\lambda\rangle$. The propagation of the state $|\Psi(t)\rangle$ was computed at least up to the time $t_{\max} = (2\Gamma_{\min})^{-1}$, where $\Gamma_{\min} \equiv \min_\lambda \text{Im } E_\lambda$ is the minimal decay rate of the complex spectrum for a given parameter set. Note that in our case the dimensionless time scale is set by the unit of time equal to $\hbar/2V$.

In Figs. 5–7 the relaxation $\langle R(t) \rangle$ of wave packets prepared with different initial energies is shown. According to Eq. (8) the initial energy E is given by $E = \sum_\lambda \text{Re } E_\lambda |e_\lambda|^2$. In parts (a) of these figures $\langle R(t) \rangle$ is shown in a semilogarithmic plot, whereas in parts (b) the spectrum of decay rates, $\Gamma_\lambda = \text{Im } E_\lambda$, and the square magnitude of the expansion coefficients from which the packet is built up, $|e_\lambda|^2$, versus the eigenstate number is displayed.

We start with a wave packet of low energy in Fig. 5. The parameters and the spectrum are as in Fig. 3. The dominant contribution to this low energy wave packet is due to expansion coefficients from eigenstates with eigenvalues in the regular part of the spectrum below the minimum of the

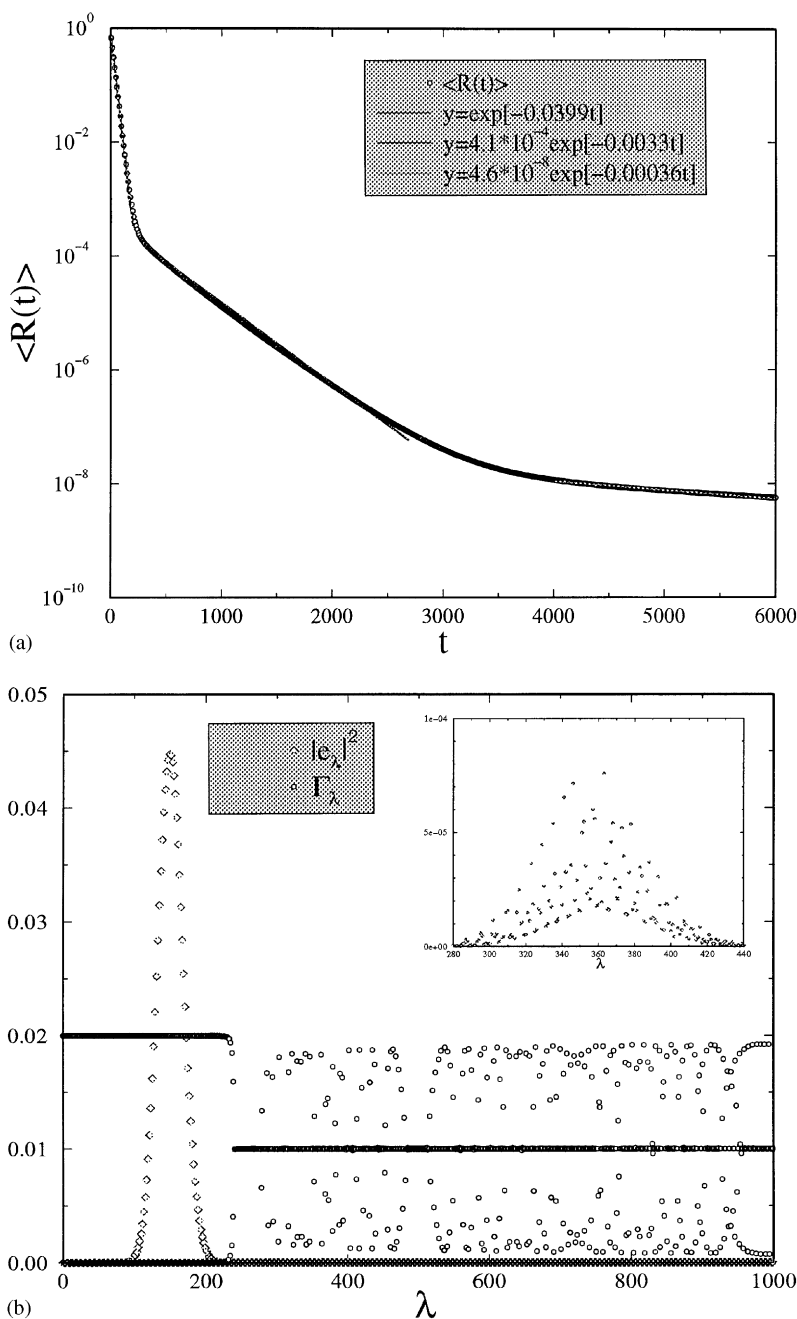
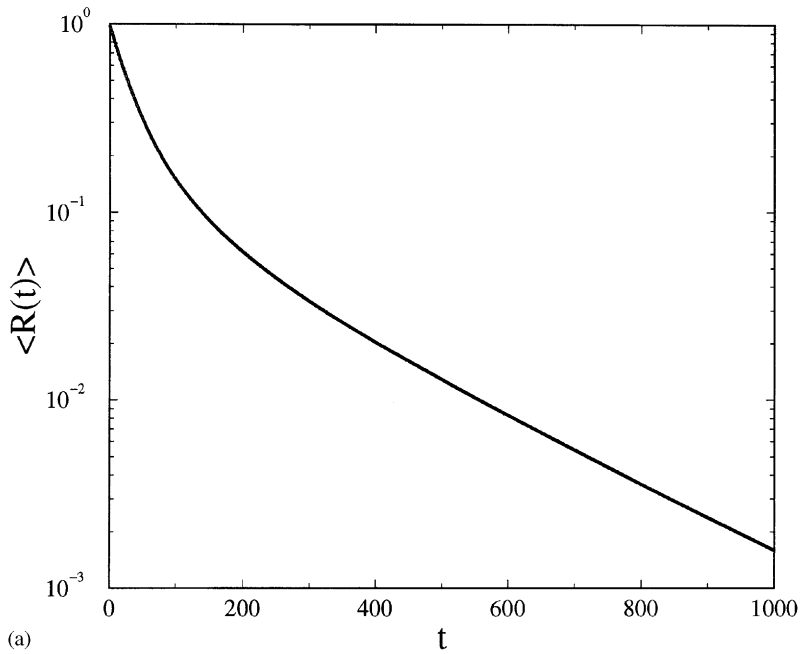
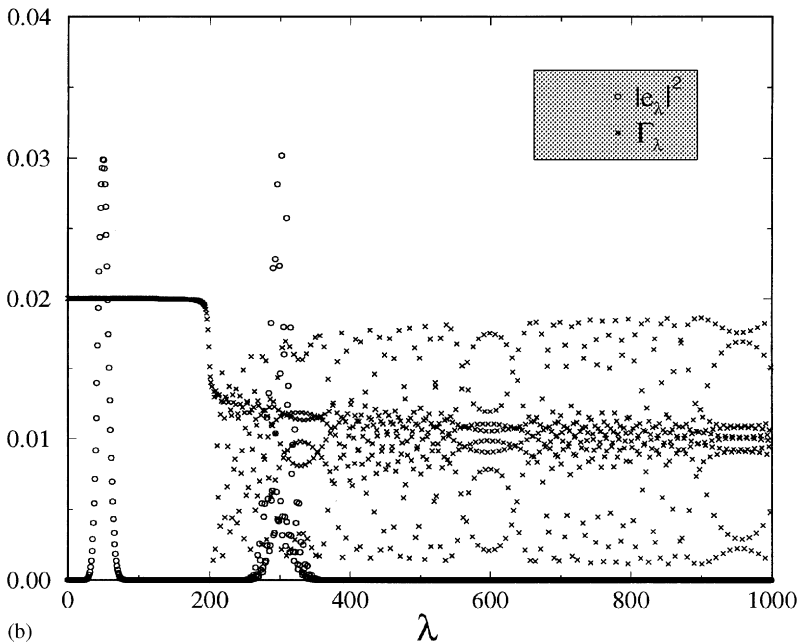


Fig. 5. Relaxation of a wave packet with a low initial energy, $\text{Re}E = -4.95$. The initial conditions are $Q = 10$, $P = 0$, $a_+ = 0$, $a_- = 1$, with the parameters as in Fig. 3. The semilogarithmic plot of the relaxation $\langle R(t) \rangle$ in (a) shows the fast and slow decay rates of the regular part of the spectrum in the short and long time behaviour of $\langle R(t) \rangle$. In between these short and long time parts there is a decay with an intermediate rate due to a small contribution of the irregular part of the spectrum in the wave packet. Exponential approximations to the three parts of $\langle R(t) \rangle$ are indicated (see legend). The eigenstates, from which the wave packet is built up, are shown as the squared expansion coefficients, $|e_\lambda|^2$, versus the eigenstate number, λ , in (b). The main contribution to the wave packet expansion is due to the regular part of the spectrum. However, there is also a small contribution from the irregular part as shown in the insert.

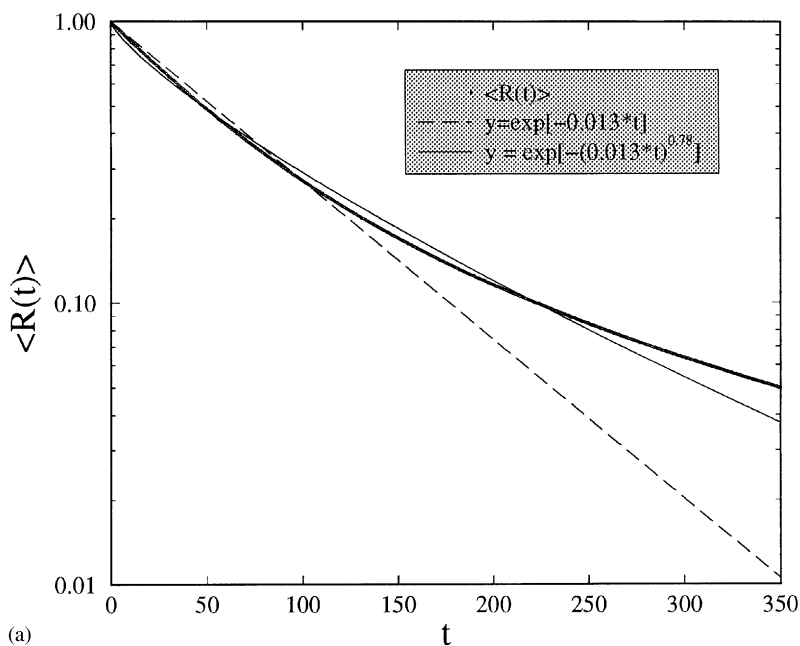


(a)

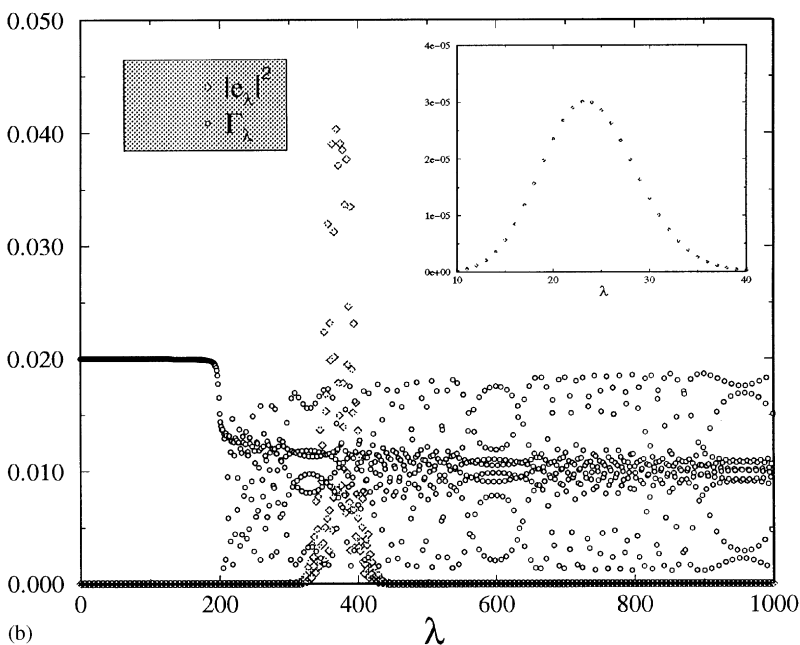


(b)

Fig. 6. Relaxation of a wave packet with an intermediate initial energy, $\text{Re}E = -0.55$. The initial conditions are $Q = 0$, $P = 0$, $a_+ = a_- = 1/\sqrt{2}$, with parameters as in Fig. 4. The relaxation $\langle R(t) \rangle$ in (a) shows a continuous flattening in the course of time. The contributions in the wave packet expansion are due to eigenstates from both the regular and irregular parts of the spectrum, as can be seen from the plot of Γ_λ and $|e_\lambda|^2$ versus the eigenstate number, λ , in (b).



(a)



(b)

Fig. 7. Relaxation of a wave packet with a high initial energy, $\text{Re}E = 13.71$. The initial conditions are $Q = 10$, $P = 0$, $a_+ = 1$, $a_- = 0$, with parameters as in Fig. 4. The relaxation $\langle R(t) \rangle$ in (a) shows a flattening which can be approximated by a stretched exponential (thin line). A simple exponential fit to $\langle R(t) \rangle$ is also shown (dashed line); (b) shows that the contributions in the wave packet expansion are due to the irregular part of the spectrum.

upper adiabatic potential (Fig. 5b). Therefore one expects a biexponential decay with a fast rate at short times and a slow rate at long times. These rates indeed show up as the straight lines in the short and long time behaviour of $\langle R(t) \rangle$ indicate (Fig. 5a). However, there is also a part with a decay intermediate between the fast and slow parts, visible in the Fig. 5a). This intermediate part is due to a small contribution from the irregular part of the spectrum which is shown in the insert of Fig. 5b). This illustrates that a low energy wave packet is not necessarily built up from states of the low energy, regular part of the spectrum only. A small weight of states from the high energy part, although not contributing significantly to the initial energy, may show up in the relaxation in the course of time.

In Fig. 6a the relaxation of a wave packet with intermediate energy is shown. The parameters are as in Fig. 4. It can be seen from Fig. 6b that now the spectrum of eigenstates which mainly build up the state vector consists of two parts with eigenvalues from both the regular and irregular parts of the spectrum. Correspondingly, we observe a decay with changing rates: Initially the relaxation $\langle R(t) \rangle$ is dominated by the fast rates of the regular part and then flattens in the course of time due to the small rates contained in the irregular part of the distribution. We note that the preparation of the initial state in this case is as in an optical low temperature excitation. In this case the oscillator packet is initially placed in the region of the vibrational ground state around $Q = 0$, there is no momentum transfer implying $P = 0$, and the light induced exciton amplitudes at the monomers are equal.

Finally, in Fig. 7a the relaxation of a wave packet of high energy is shown. It is obtained by selecting an initially displaced wave packet at $Q = 10$. The parameters are as in Fig. 6, but now the packet is mainly built up from the irregular part of the decay rate spectrum only, as shown in Fig. 7b. Accordingly we observe a relaxation $\langle R(t) \rangle$ shifting continuously from faster to slower decay rates. In Fig. 7a we also present a fit of $\langle R(t) \rangle$ by a stretched exponential of the form $\langle R(t) \rangle = \exp[-(at)^p]$. It is seen that most part of the decay is well represented by this dependence

with $p = 0.78 < 1$. In regard to this we point out an analogy to anomalous relaxation in disordered systems, where stretched exponential decay is familiar (see, e.g. Ref. [7]). In a disordered system such a decay is due to e.g. luminescence quenching in a random environment of excitation traps. In the present case the origin of the distribution of decay rates is completely different and it is an intrinsic property of the quantum states.

4. Conclusions

Finite lifetimes of excited states of the monomers in an asymmetric dimer with a strong excitonic–vibronic coupling can give rise to a broad distribution of relaxation rates. As a consequence different relaxation behaviour may arise ranging from near biexponential decay to decays approximated by stretched exponential like dependences. The results should be of interest from an experimental point of view, for time resolved luminescence experiments at low enough temperatures, when the strong coupling of the excitation to a single vibrational mode dominates over temperature related bath effects.

Acknowledgements

The authors would like to thank Holger Schanz for useful discussions.

References

- [1] P. Reineker, Stochastic Liouville equation approach, in: *Molecular Crystals and Aggregates*, Springer Tracts in Modern Physics, vol. 94, Springer, Berlin, 1982, p. 111.
- [2] V. Szócs, P. Baňacký, *Chem. Phys.* 186 (1994) 153.
- [3] H. Schanz, B. Esser, *Phys. Rev. A* 55 (1997) 3375.
- [4] R. Steib, J.L. Schoendorff, H.J. Korsch, P. Reineker, *J. Lumin.* 76 & 77 (1998) 595.
- [5] B. Esser, H. Schanz, *Z. Phys. B* 96 (1995) 553.
- [6] U. Rempel, B. von Maltzan, C. von Borczyskowski, *J. Lumin.* 53 (1992) 175.
- [7] A. Blumen, J. Klafter, G. Zumofen, *Models for reaction dynamics in Glasses*, in: I. Zschokke (Ed.), *Optical Spectroscopy of Glasses*, Reide, Dordrecht, 1986, p. 199.
- [8] H. Schanz, B. Esser, *J. Lumin.* 76 & 77 (1998) 530.